temperature is simply to average $\Delta t(\varepsilon)$ over energy, the more complex behavior of the I_{net} allows us to observe current reversals in both directions in the experiment (Fig. 2A). In close agreement between experiment and model, the temperature at which reversal occurs is typically a few kelvin, a value that is related to the energy scale of variations of $\Delta t(\varepsilon)$ (Fig. 3). The observed I_{net} exceeds that found in the model, indicating that the voltage-induced modification of the ratchet potential is stronger than what is assumed in the calculation. Although a rigorous theoretical treatment will be of interest (*24*), the 1D single-barrier model used here yields intuitive, qualitative understanding of the sign and temperature dependence of the observed net current.

The observation that the rocking-induced flow of electrons with high and low energy is in opposite directions (Fig. 3) has a fundamentally interesting implication: A tunneling ratchet can perform the energy-sorting task assigned to Maxwell's demon (*27*), without violating the second law of thermodynamics, because it operates only at a finite voltage. Another important aspect is that artificial nanostructures can be used to test physical principles that may be of importance in living systems. Whether transport mechanisms based on quantum effects such as the one studied here play a role in biological motor proteins is an intriguing question.

References and Notes

1. M. O. Magnasco, *Phys. Rev. Lett.* **71**, 1477 (1993).
2. J. Prost, J.-F. Chauwin, L. Peliti, A. Ajdari, *Phys. Rev. Lett.* **72**, 2652 (1994).
3. C. R. Doering, W. Horsthemke, J. Riordan, *Phys. Rev. Lett.* **72**, 2984 (1994).
4. P. Hänggi and R. Bartussek, in *Nonlinear Physics of Complex Systems—Current Status and Future Trends*, J. Parisi, S. C. Müller, W. Zimmermann, Eds. (Springer, Berlin, 1996), pp. 294–308.
5. R. D. Astumian, *Science* **276**, 917 (1997).
6. S. Leibler, *Nature* **370**, 412 (1994).
7. F. Jülicher, A. Ajdari, J. Prost, *Rev. Mod. Phys.* **69**, 1269 (1997).
8. J. Maddox, *Nature* **369**, 181 (1994).
9. K. Kitamura, M. Tokunaga, A. H. Iwane, T. Yanagida, *Nature* **397**, 129 (1999).
10. J. Rousselet, L. Salome, A. Ajdari, J. Prost, *Nature* **370**, 446 (1994).
11. L. P. Faucheux, L. S. Bourdieu, P. D. Kaplan, A. J. Libchaber, *Phys. Rev. Lett.* **74**, 1504 (1995).
12. L. Gorre, E. Ioannidis, P. Silberzan, *Europhys. Lett.* **33**, 267 (1996).
13. H. Linke *et al.*, *Europhys. Lett.* **44**, 341 (1998); H. Linke *et al.*, *Europhys. Lett.* **45**, 406 (1999).
14. A. Lorke *et al.*, *Physica B* **251**, 312 (1998).
15. C. Mennerat-Robilliard *et al.*, *Phys. Rev. Lett.* **82**, 851 (1999).
16. X. Wang, T. Junno, S.-B. Carlsson, C. Thelander, L. Samuelson, available at http://xxx.lanl.gov/abs/cond-mat/9910444.
17. P. Reimann, M. Grifoni, P. Hänggi, *Phys. Rev. Lett.* **79**, 10 (1997).
18. I. Goychuk and P. Hänggi, *Europhys. Lett.* **43**, 503 (1998).
19. P. Hänggi and P. Reimann, *Phys. World* **12**, 21 (March 1999).
20. In addition, to remove any contributions to I_{net} not related to the asymmetry of the device, each experimental sweep was carried out in forward and reverse configuration of the device, and the two data sets were added.
21. One-dimensional quantum conduction theory is reviewed by S. Datta, *Electronic Transport in Mesoscopic Systems* (Cambridge Univ. Press, Cambridge, 1995).
22. In the sign convention used here, positive electrical current corresponds to an electron particle current in negative x direction.
23. H. Xu, *Phys. Rev. B* **47**, 15630 (1993).
24. A rigorous theory of nonlinear quantum transport requires self-consistent treatment of the electrostatic device potential at finite voltage based on the three-dimensional Schrödinger equation.
25. C. W. J. Beenakker and H. van Houten, *Phys. Rev. B* **39**, 10445 (1989).
26. A. A. M. Staring, L. W. Molenkamp, C. W. J. Beenakker, L. P. Kouwenhoven, C. T. Foxon, *Phys. Rev. B* **41**, 8461 (1990).
27. For a collection of key articles, see, for example, H. S. Leff and A. F. Rex, *Maxwell's Demon: Entropy, Information, Computing* (IOP, Bristol, UK, 1990).

28. We acknowledge helpful discussions with P. Reimann, P. Stiles, M. Stopa, O. Sushkov, and H. Xu and technical help by M. Alat, W. D. Sheng, and X. Wang. Supported by the Australian Research Council, the Swedish Research Council for Natural Sciences, the Foundation of Strategic Research, and by a travel grant from the Swedish Institute (A.L.).

26 August 1999; accepted 28 October 1999

Three-Dimensional Atomic-Scale Imaging of Impurity Segregation to Line Defects

D. Blavette,* E. Cadel, A. Fraczkiewicz,† A. Menand

Clouds of impurity atoms near line defects are believed to affect the plastic deformation of alloys. Three-dimensional atom probe techniques were used to image these so-called Cottrell atmospheres directly. Ordered iron-aluminum alloys (40 atomic percent aluminum) doped with boron (400 atomic parts per million) were investigated on an atomic scale along the ⟨001⟩ direction. A boron enrichment was observed in the vicinity of an ⟨001⟩ edge dislocation. The enriched region appeared as a three-dimensional pipe 5 nanometers in diameter, tangent to the dislocation line. The dislocation was found to be boron-enriched by a factor of 50 (2 atomic percent) relative to the bulk. The local boron enrichment is accompanied by a strong aluminum depletion of 20 atomic percent.

The concept of "atmospheres" was introduced by Cottrell and Bilby (*1*) in 1949 to explain the role of impurities in the plastic deformation of alloys. These so-called Cottrell atmospheres are tiny clouds of impurity atoms around dislocations in crystals. These line defects play a major role in the plasticity of materials. The geometry of an edge dislocation is described by an extra half-plane inserted into the lattice (Fig. 1). The locus where the half-plane terminates is the dislocation line. Such a dislocation gives rise to an elastic distortion of the lattice around the line of the defect, and consequently to a stress field with which solute impurities may interact. Interstitial impurities such as carbon or boron cause a deformation of the lattice, which may be partially released if these elements segregate near line defects. The stress field created by dislocations is the driving force for the migration of solutes toward dislocations. Interstitial impurities (or oversized atoms in substitution) generally segregate in the dilated part of edge dislocations, below the dislocation line, whereas undersized substitutional atoms are likely to migrate toward the compressed regions above slip planes. This stress-induced migration therefore leads to the segregation of solutes along dislocation lines and to the formation of solute-enriched regions, the Cottrell atmospheres. Their extent, as estimated from diffusion arguments, is in the nanometer range. Cottrell atmospheres play a major role in the mechanical properties of materials. Their presence may inhibit the movement of dislocations, which are "pinned" by the solute atmospheres. If temperatures are high enough to permit appreciable diffusion, dynamic strain aging may occur during deformation. These so-called Portevin-LeChatelier instabilities are due to the pinning of freshly formed dislocations by new atmospheres that form during deformation. Such dynamic effects have been reported in a number of steels (*1*).

Direct evidence for these atmospheres is extremely rare because of the very high spatial resolution required. Atom-probe field ion microscopy (APFIM) is the most promising technique for this kind of investigation because it

Sonde Atomique et Microstructures, Groupe de Métallurgie Physique, UMR CNRS 6634, Faculté des Sciences de Rouen, Université de Rouen, 76821 Mont-Saint-Aignan Cedex, France.

*To whom correspondence should be addressed. E-mail: blavette@univ-rouen.fr

†Ecole des Mines de Saint-Etienne, Centre SMS, 158 Cours Fauriel, 42 100 Saint-Etienne, France.

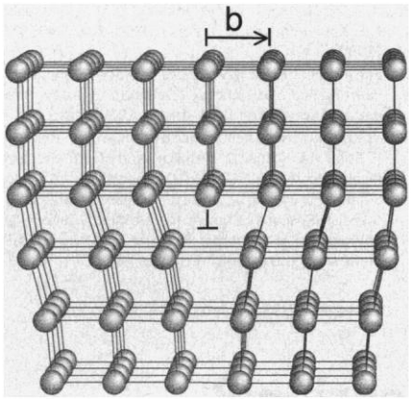

Fig. 1. Schematic representation of an ⟨001⟩ edge dislocation in a cubic lattice. The dislocation line terminates the extra half-plane (⊥). The Burgers vector **b** is perpendicular to the dislocation line. Impurities are expected to segregate along the dislocation line, in the distorted region of the crystal. This dislocation can move along a slip plane parallel to **b** and the line defect.

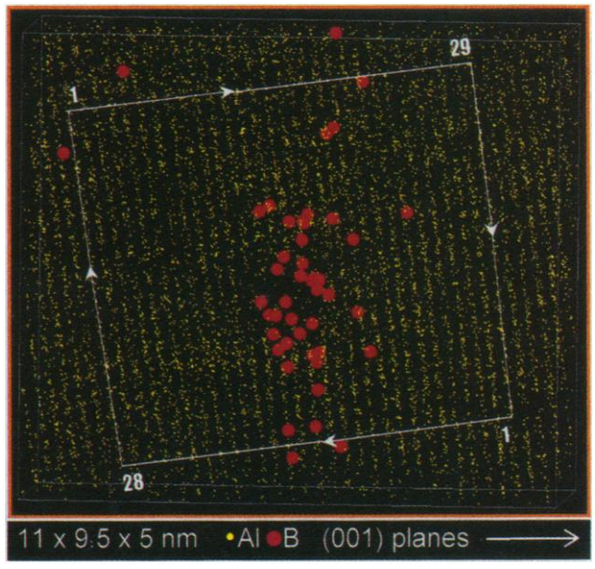

Fig. 3. Top view of Fig. 2. This 3D image is a small slice perpendicular to the boron rod shown in Fig. 2. The area visualized is 11 nm by 9.5 nm. The third dimension of the reconstructed volume (almost perpendicular to the figure) is 5 nm. Imaged planes, separated by 0.29 nm, are almost perpendicular to the ⟨001⟩ depth axis. Maps of aluminum (green) and boron (red) show the presence of a boron-enriched Cottrell atmosphere along an edge dislocation. The Burgers circuit indicates the presence of an edge dislocation, which is thought to be above the center of the atmosphere. The dislocation line is perpendicular to the image, and the Burgers vector is perpendicular to Al-rich (001) planes (see Fig. 1).

combines atomic-scale resolution with quantitative chemical analysis (*2*). One of the first APFIM observations of atmospheres in iron was carried out by Chang *et al.* (*3*) in low-carbon martensites. However, this study was only two-dimensional (2D), and because the dislocation could not be displayed in three dimensions, the distribution of solutes along the line could not be shown. Cottrell atmospheres were also analyzed using 1D APFIM in NiAl intermetallics containing Zr and Hf (*4*). Again, no 3D information on the atmosphere was given.

Here, a solute atmosphere around an edge dislocation was observed and analyzed on the atomic scale in three dimensions. Three-dimensional atom probe (3DAP) techniques (*5, 6*) were used to investigate such atmospheres in boron-doped FeAl intermetallics. Boron improves mechanical resistance through a reinforcement of grain boundaries (*7*), and boron is known to segregate to grain boundaries (*8*). We investigated FeAl alloys that contained 40 atomic % Al and 400 atomic ppm of boron. They were subjected to a two-step treatment: 950°C for 1 hour (quenching), then 400°C for 24 hours (air cooling). This treatment gave rise to a well-ordered B2 structure (*9*). Iron preferentially occupies the corners, and Al the centers, within the body-centered cubic cell. The boron concentration is below the solubility limit, which has been estimated to range between 400 and 800 ppm (*8*). The second stage of treatment at 400°C eliminates a large proportion of vacancies retained after quenching from 950°C. The elimination of vacancy in excess at 400°C is known to give rise to the formation of dislocations, mainly of ⟨100⟩ Burgers vector (*10*).

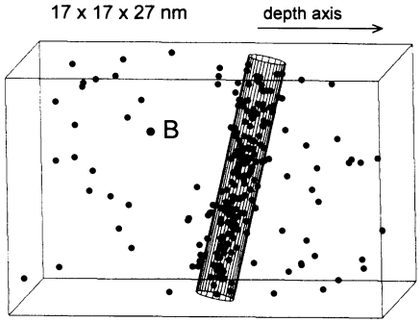

Fig. 2. A 3DAP image showing the presence of a boron-enriched atmosphere in B2-ordered FeAl intermetallics. Only boron atoms are represented; Fe and Al are omitted for clarity. The cylindrical envelope illustrates the rod-like morphology of the boron-enriched atmosphere. Boron segregates along a direction, ⟨100⟩, parallel to the dislocation line shown in Fig. 3. The analysis started on the left side, and the volume was reconstructed layer by layer along the depth axis. The analyzed area is a square, 17 nm by 17 nm.

We used 3DAP together with field ion microscopy (FIM) to determine the atomic-scale distribution of chemical species around lattice defects. This technique can map the 3D distribution of chemical species with a depth resolution of a single atomic layer. An electric field induces ions to evaporate from a needle-like surface; these ions are then identified by time-of-flight mass spectrometry (*2*). A position-sensitive detector is used to determine the position of incoming ions and their initial location at the specimen surface. The material is field-evaporated at low temperatures (70 K in our experiments), layer by layer, so that the small volume that is analyzed (15 nm by 15 nm by 100 nm) can be reconstructed in 3D on a near-atomic scale. Standard electropolishing procedures were used to prepare specimens in the form of sharply pointed needles (*2*). Experiments were conducted along the ⟨001⟩ direction to detect ⟨001⟩ dislocations present in the material. Technical details are provided in (*9*). Because of the small distances that can be probed with 3DAP relative to the mean dislocation spacing (100 nm versus 1 μm) and the heterogeneous distribution of dislocations within the material, numerous experiments were necessary before a decorated dislocation could be analyzed.

A 3D reconstruction (Fig. 2) shows the presence of a boron (B) enrichment within the small volume that was analyzed. This enrichment appears as a pipe aligned along the ⟨100⟩ crystallographic direction. This orientation could be established from the orientation of the detection area with respect to zone axes in FIM images.

This B-enriched cloud is shown in a more detailed way in Fig. 3, a top view oriented parallel to the (001) planes. The axis of the B-enriched pipe is perpendicular to the figure plane. The ultrahigh resolution of 3DAP makes it possible to image the stacking sequence of the superlattice (001) planes of this ordered material. As expected for a B2-ordered structure, Al-enriched planes alternate with Al-depleted (that is, Fe-enriched) planes.

By counting the number of imaged planes in the region limited by the white line, it is easy to see that an extra half-plane is present in the top part of the zone (Fig. 3). The dislocation line is perpendicular to the figure and parallel to the ⟨100⟩ direction. The construction of the so-called Burgers circuit (white line) shows that an edge dislocation is present. The Burgers vector **b** is defined as the vector that closes the Burgers circuit; **b** is parallel to ⟨001⟩ and its length is equal to the lattice parameter of the crystal (Fig. 3). This dislocation is therefore a perfect $a\langle 001\rangle$ dislocation of B2-ordered FeAl. Note also the

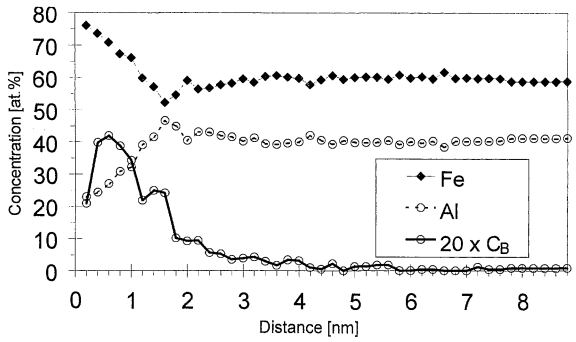

Fig. 4. Radial distributions of Fe, Al, and B (concentration in atomic percent, multiplied by 20 for boron) with respect to the center of the boron atmosphere. Boron segregation extends up to 3 nm from the dislocation core. Calculated concentrations (C) are subject to sampling errors, which gradually decrease with r according to the relation $\delta C \sim [C(1 - C)/N]^{1/2}$, where the number of ions (N) is proportional to r^2. The statistical fluctuations related to the maximum boron concentration (2 atomic %) are close to 1 atomic %.

local curvature of planes in the close vicinity of the end of the extra half-plane, in good agreement with geometrical descriptions of edge dislocations.

The B-enriched pipe-shaped zone, parallel to the dislocation line, is detected in the vicinity of the extremity of the additional half-plane (Fig. 3). This image therefore provides evidence that the B-enriched zone shown in Fig. 2 is a Cottrell atmosphere. Interstitial atoms like boron are likely to segregate under the dislocation line, in the dilated region of the defect. Therefore, a plausible location of the dislocation could be around 1 nm above the center of the atmosphere (Fig. 3). However, the exact location of the dislocation line in the reconstructed image is difficult to ascertain with certainty.

The position of the B-rich pipe, slightly to the right of the apparent position of the dislocation line, is a priori surprising. However, reconstructed images must be interpreted with caution. The applied stress caused by the high electric field may have led to a partial breakaway of the dislocation from its atmosphere during the investigation, resulting in a shift of the line defect by a few atomic planes toward the specimen surface (left side, Figs. 2 and 3). Preferential retention of boron from one plane to the next may also shift boron slightly (0.15 nm) to the left in Fig. 3.

Radial distributions of atomic species (Fig. 4) with respect to the center of mass of the atmosphere (that is, the axis of the boron "finger" shown in Fig. 2) were calculated in successive shells of equal thickness (0.2 nm). The maximum concentration of boron C_B is close to 2 atomic %. The extent of the atmosphere, taken at one-tenth of the maximum boron concentration (that is, $C_B = 0.2$ atomic %), can be estimated at 3 nm.

In a first approximation, the interstitial concentration C_B at a given temperature T in the strain field of a dislocation can be written as $C_B = C^0 \exp(u/kT)$, where C^0 is the nominal boron concentration (400 atomic ppm), u is the binding energy between the dislocation and interstitial, and k is the Boltzmann constant. From the present measurements we estimate $u \approx 0.2$ eV, a reasonable value compared to the binding energy of carbon in iron (~0.5 eV). [A more detailed interpretation using recent models (*11, 12*) has not yet been offered.] One feature in Fig. 4 is unexpected: The Al concentration falls at the center of the atmosphere (20 atomic %, as compared to 40 atomic % in the bulk).

Similar atmospheres were encountered during the systematic experiments that were carried out. Among the three boron-enriched clouds that could be found, only one could be interpreted quantitatively on a sound basis. This atmosphere appeared as a rod-shaped zone containing 6 atomic % boron. Similar to what is shown in Fig. 4, the boron-enriched zone was Al-depleted (33 atomic %). Its diameter was close to 3 nm. Unfortunately, the dislocation line associated with this atmosphere could not be imaged.

The information revealed by 3DAP on the spatial distribution of chemical species near line defects is important both from an academic point of view and for applications. The observed modifications of concentrations close to dislocation lines evidently alter the core structure of defects, which in turn has a great influence on the plasticity behavior of material. The existence of the unexpected Al depletion within Cottrell atmospheres is an intriguing phenomenon that remains to be explained.

References

1. A. H. Cottrell and B. A. Bilby, *Proc. Phys. Soc. London Ser. A* **62**, 49 (1949).
2. M. K. Miller, A. Cerezo, M. G. Hetherington, G. D. W. Smith, *Atom Probe Field Ion Microscopy* (Clarendon, Oxford, 1996).
3. L. Chang, S. J. Barnard, G. D. W. Smith, in *Fundamentals of Aging and Tempering in Bainitic and Martensitic Steel Products*, G. Klaus and P. E. Repas, Eds. (Iron & Steel Society, Warrendale, PA, 1992), pp. 19–28.
4. R. Jayaram and M. K. Miller, *Scr. Metall. Mater.* **33**, 19 (1995).
5. D. Blavette, A. Bostel, J. M. Sarrau, B. Deconihout, A. Menand, *Nature* **363**, 432 (1993).
6. A. Cerezo, T. J. Godfrey, G. D. W. Smith, *Rev. Sci. Instrum.* **59**, 862 (1988).
7. M. A. Crimp and K. Vedula, *Mat. Sci. Eng.* **78**, 193 (1986).
8. A. Fraczkiewicz, A.-S. Gay, M. Biscondi, *J. Phys. IV* **9**, 75 (1999).
9. D. Blavette, B. Deconihout, S. Chambreland, A. Bostel, *Ultramicroscopy* **70**, 115 (1998).
10. M. A. Morris and D. G. Morris, *Scr. Metall. Mater.* **38**, 509 (1998).
11. A. S. Nandedkar and R. A. Johnson, *Acta Met.* **30**, 2055 (1982).
12. W. G. Wolfer and M. I. Baskes, *Acta Met.* **33**, 2005 (1985).

6 September 1999; accepted 10 November 1999

Deflection of the Local Interstellar Dust Flow by Solar Radiation Pressure

M. Landgraf,[1,2]* K. Augustsson,[3] E. Grün,[4] B. Å. S. Gustafson[5]

Interstellar dust grains intercepted by the dust detectors on the Ulysses and Galileo spacecrafts at heliocentric distances from 2 to 4 astronomical units show a deficit of grains with masses from 1×10^{-17} to 3×10^{-16} kilograms relative to grains intercepted outside 4 astronomical units. To divert grains out of the 2– to 4–astronomical unit region, the solar radiation pressure must be 1.4 to 1.8 times the force of solar gravity. These figures are consistent with the optical properties of spherical or elongated grains that consist of astronomical silicates or organic refractory material. Pure graphite grains with diameters of 0.2 to 0.4 micrometer experience a solar radiation pressure force as much as twice the force of solar gravity.

Identical dust impact detectors (*1, 2*) were installed on the Ulysses spacecraft, which flies in a polar orbit around the sun, and on the Galileo spacecraft, which continues to fly in a jovian orbit. The instruments sense the plasma cloud generated as individual dust grains strike a detector plate at high velocity. Independent impact plasma charge measurements distinguish real events from spurious recordings and were used to derive the grain mass and impact velocity (*3*).

The Ulysses and Galileo dust measurements were mainly designed to reveal the spatial distribution of interplanetary dust grains that are released from minor solar system objects like asteroids and comets (*4*).